Molecular dynamics simulations of ion transport through carbon nanotubes. II. Structural effects of the nanotube radius, solute concentration, and applied electric fields

Titus A. Beu[a)]
Faculty of Physics, University "Babeş -Bolyai," 400084 Cluj-Napoca, Romania

(Received 17 February 2011; accepted 6 July 2011; published online 29 July 2011)

The reported work extends previously published research on transport in aqueous ionic solutions through carbon nanotubes. Specifically, the effects of the nanotube radius, solute concentration, and applied external electric fields on the solution structuring are investigated in terms of spatial density distributions, pair distribution functions, and electrostatic potential profiles. Several simulated structural features are consistent with general theoretical results of nanofluidics and can be interpreted fairly well with respect to these (such as the Donnan-type voltages established at the channel apertures depending on the logarithm of the maximum ion concentration). The simulated properties are based on averages over the largest data collection times reported in the literature (0.8 μs), providing accurate estimates of the measured quantities. © *2011 American Institute of Physics*. [doi:10.1063/1.3615727]

I. INTRODUCTION

Almost two decades after their discovery,[1] carbon nanotubes (CNTs) continue to attract considerable interest due to their exceptional properties and yet emerging applications.[2] The unexpectedly high flow rates, mostly independent of the pore length, turn single-walled CNTs into promising materials for nanofluidic technology, opening perspectives to applications involving filtration and separation. A great deal of research has been also devoted to the theoretical modeling and prediction of various features of the CNTs. A comprehensive review of the present status and outlook concerning the water in nonpolar confinement, ranging from nanotubes to proteins, was published recently by Rasaiah *et al*.[3]

The present paper is the second in a series dedicated to the systematic study by atomistic molecular dynamics (MD) simulations of the ion transport through "armchair"-type (n, n) CNTs of chiralities ranging from (8,8) to (12,12) (radii from 5.42 to 8.12 Å) filled with NaCl and NaI solutions.

In our first paper,[4] hitherto referred to as Paper I, the dependences of diverse transport features on the solute specificity, the nanotube geometry, and the various atomic models employed have been addressed in detail and interpreted in their interdependence with the solution structuring and the energy barriers faced by the solute components. Also, an in-depth analysis of the relevance of the water and ion polarizabilities was developed.

The simulations reported in Paper I show that the detailed molecular structure of the solution inside the nanopore is crucial to understanding the ion permeation process. The results are consistent with those from the literature,[5–11] confirming that ions face significant energy barriers and are able to pass only through CNTs with chiralities higher than (7,7).

The solution appears to be highly structured in the vicinity of the carbon walls, featuring similar and almost invariant radial and axial patterns, independent of the CNT size. The cylindrical (planar) water layers formed inside the channel (at the membrane) enclose alternating regions of peaking solute ion density. The water boundary layer is located independently of the solute type, pore radius, and polarizability, at a distance of roughly 3.2 Å from the carbon walls and the densities of the I^- and Na^+ ions peak invariably at about 4.1 and, respectively, 5.0 Å. A similar radial structuring was described in several of the above cited papers and, more recently, inside statically filled CNTs.[12]

Inside the wider CNTs the axial profiles of the potential of mean force are almost flat and ion non-specific, the ion motion appearing to be frictionless. The narrow (8,8) CNT, however, exhibits ion-dependent free energy barriers with non-vanishing slopes, implying less probable translocations and, in particular, a certain ion specificity determined by a slightly lower free energy barrier for I^- as compared to Cl^-. The average potential barriers faced by the ions to enter the pore are significantly higher than the voltage between the channel ends caused just by the applied electric field and decrease with increasing pore radius, being a consequence of the electrical double layers formed at the membrane walls.

The translocation dynamics of the solute ions has been shown in Paper I to have a strong pore radius dependence. The ionic current profiles are roughly parabolic and vanish practically for the narrowest of the considered nanopores (8,8), the overall behavior being consistent with other calculations.[5–8] Notably, a distinct selectivity of the CNTs with respect to the anion species can be identified, the total currents for the NaI solution exceeding on average by 30% the ones for the NaCl solution. This finding is consistent with the differences in the radial structuring of the solution inside the pores (the I^- anions transiting the CNTs via cylindrical flux layers of larger

a)Electronic mail: titus.beu@phys.ubbcluj.ro.

average radius) and further arguments are the lower free energy barrier and the shorter passage times through the pore for I^- as compared to Cl^-. With decreasing ion mass, the ion passage times increase, the light Na^+ ions experiencing the slowest and most sinuous translocations.

Even though polarizable interaction models have been demonstrated in Paper I to increase the I^- density in the proximity of the water boundary layers, the density peak positions as such are not affected. Moreover, polarizability appears to have a negligible impact on the ion currents, indicating that extensive nanofluidics simulations of dynamic quantities can be carried out accurately disregarding costly polarizable models.

The present work focuses in particular on the effects of the solute concentration and applied external electric fields on the *solution structuring* inside CNTs. The main structural quantities analyzed are the density profiles and pore/reservoir density ratios of the solution components, their pair distribution functions and coordinations, as well as the water polarization and electrostatic potential. In addition, certain dependences on the CNT radius (as, for instance, pair distribution functions and coordinations) are also presented, complementing the information reported in Paper I. The relevant ensemble-averaged quantities are based on the longest data collection times reported so far for atomistic simulations of flows through CNTs (0.8 μs), ensuring high accuracy of the measured quantities.

The influences of the solute concentration and applied external electric fields on the *transport* of the NaCl and NaI solution components through CNTs are discussed at length in the next paper[13] in terms of diffusion coefficients, ion currents, drift mobilities, and ion pairing times. Correlations between the structural and dynamic properties are established, linking causally the radial density profiles and the ion pairing phenomenon with the ionic currents and charge carrier mobilities. Discontinuities in the partial ionic currents are explained on the basis of a recent theoretical model of quantized ionic conductance in nanopores, developed by Zwolak and co-workers.[10,11]

II. SIMULATION DETAILS

Similar to Paper I, the simulations reported here have been performed entirely by a homemade computer code (MDsquad). Among the distinctive modeling aspects, a central role is played by the usage of rigid-body dynamics for the water molecules in conjunction with site-site interaction models, which assure appreciable accuracy on the μs time scale of interest.

The MD integrator employed both for the translational and rotational degrees of freedom is a forth order Gear-type predictor-corrector algorithm.[14] The initial equilibration runs have been performed with a time step of 1 fs to overcome the instabilities caused by the large initial density gradients. Nevertheless, for the massive production runs, 2.5 fs was shown in Paper I to be a small enough time step to ensure the desired accuracy, still maintaining the very demanding simulations tractable. A Gaussian thermostat,[14] known for conserving the velocity distributions, is implemented for the translational degrees of freedom of the water molecules; whereas the remaining degrees of freedom are allowed to relax freely to the equilibrium temperature.

In order to eliminate surface effects and to ensure continuous flows through the CNTs, periodic boundary conditions in all three Cartesian directions are applied. Additionally, to account accurately for the long-range electrostatic interactions of the charges and their periodic images, Ewald sum techniques are employed. The usage of the P^3M particle-particle/particle-mesh Ewald method developed by Hockney and Eastwood,[15] as formulated by Deserno and Holm,[16] makes extensive simulations over sufficiently long time intervals possible, allowing for reliable current flows to be measured. Details on the electrostatics are provided in Paper I.

The molecular representation used for water throughout in the present work has been the non-polarizable four-site model TIP4P of Jorgensen and co-workers.[17,18] The polarizable five-site model COS/G2 of Yu and van Gunsteren[19] employed in Paper I to assess the relevance of molecular polarizability was no longer used since; whereas it was shown to enhance the average accumulation of ions at the carbon walls, it turned out to produce effects neither on the density peak positions nor on the translocation dynamics. For the same reason, the polarizability of ions has been disregarded in the current paper as well.

As solute anions, we have selected two representative halides from the Hofmeister series, i.e., chloride and iodide, which are known to have a different enough behavior to suggest general trends within the series. All relevant geometry and interaction parameters for the employed water and ion models are summarized in Paper I.

The channel model consists of a rigid non-polar "armchair"-type (n, n) CNT of length 60.17 Å extending symmetrically between two neutral graphene planes and two reservoirs on either side.[4] The size of the simulation cell containing the system has been adjusted in all cases such as to produce for 1000 water molecules a density of 1 g/cm^3 relative to the accessible volume. Ion concentrations from ~0.28M to 1.66M have been considered, resulting from 10, 20, 30, 40, 50, and, respectively, 60 ions of both species. In order to drive the ions through the channel, homogeneous electric fields of 0.005, 0.01, 0.02, 0.03, 0.04, and 0.05 V/Å have been applied parallel to the channel axis.

For each particular solute type, nanotube radius, ion concentration, and applied electric field, a total evolution time of 0.8 μs (double, compared to Paper I) was simulated with a time step of 2.5 fs at constant temperature ($T = 300$ K). With a view to reduce time correlations and improve statistics by better sampling the phase space, the measurements have been compiled from *NVT* ensembles of 64 trajectories of 12.5 ns, each started from a different random initial configuration. The preparation of the initial configurations has been accomplished by starting from an originally empty channel between densely filled reservoirs and allowing for the subsequent relaxation of the solution inside the channel and the equilibration of the system for 1 ns.

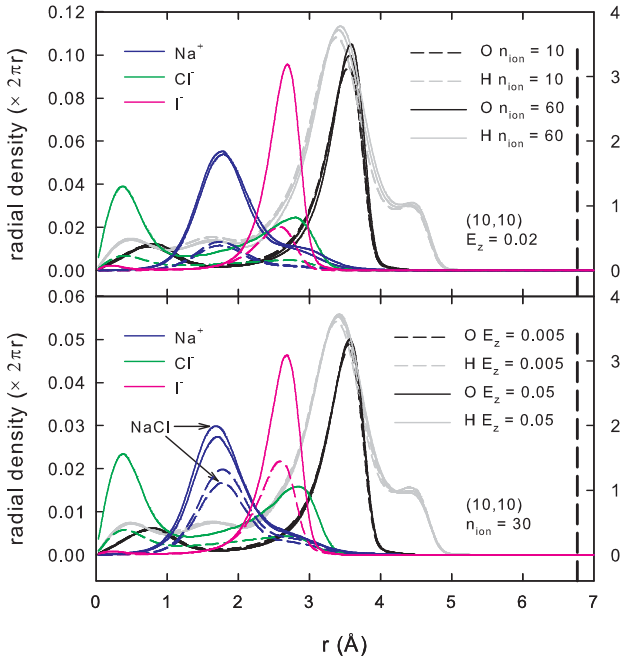

FIG. 1. Axially averaged radial density profiles for water and ions inside the CNT (10,10) for representative solute ion concentrations (upper panel) and axial electric fields (lower panel). Dashed lines correspond to the lower parameter value. The left vertical scales refer to the ions and those on the right, to the water components. The dashed drop-lines indicate the position of the carbon wall.

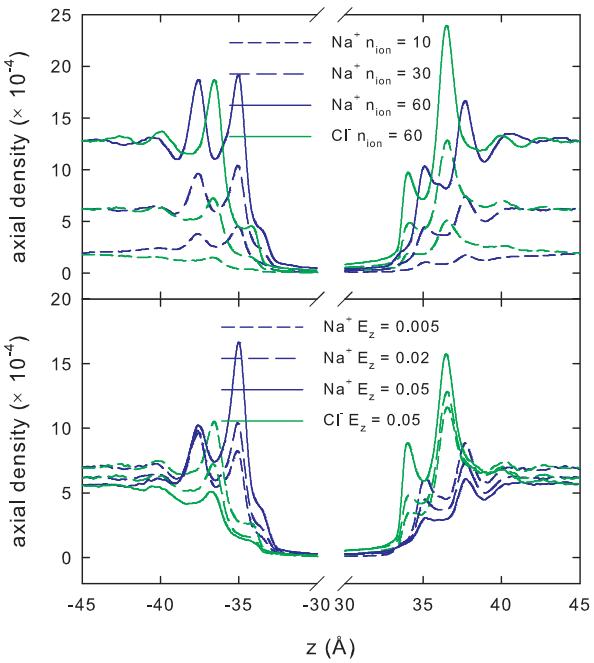

FIG. 2. Transversally averaged axial density profiles for Na^+ and Cl^- for the CNT (10,10) for representative total numbers of ions (upper panel) and axial electric fields (lower panel). The pore region is excluded.

III. RESULTS AND DISCUSSION

A. Solution structuring

As basic information produced by the simulations, the ensemble-averaged radial density profiles for water and ions provide a detailed picture on the average solution structuring inside the pores and, in particular, in the proximity of the carbon walls. For the reference case of the CNT (10,10), these profiles are plotted in Fig. 1 for representative solute ion concentrations and selected axial electric fields. Similar plots, however for 30 ions (15 Na^+ cations and 15 anions) and for an axial electric field of 0.02 V/Å have been presented in Paper I for the CNTs of chiralities (8,8), (10,10), and (12,12). The same color scheme is maintained and, in addition, the symbols used in subsequent plots are circles for the NaCl solution and squares for the NaI solution.

As a difference from Paper I, in which the radial density profiles for water referred to the center-of-mass of the molecules, in order to suggest also the average relative orientation of the molecules, implicitly giving information about the hydration of the ions, in Fig. 1 separate profiles for oxygen (black lines) and hydrogen (grey lines) have been included. The profiles are averaged over the effective pore length $2z^{\text{eff}}_{\text{pore}} = 63.52$ Å ($z^{\text{eff}}_{\text{pore}} = z_{\text{pore}} + \sigma_{\text{graph}}$, $\sigma_{\text{graph}} = 1.674$ Å is half the graphite inter-plane distance) and, being obtained by direct binning of the radial positions of the solution components, they include implicitly the angular integration factor $2\pi r$.

Consistently with the findings of Paper I and of the related literature, regardless of the pore radius, applied electric field, or solute concentration, water forms well-defined boundary layers both inside the channel and near the membrane surfaces. These density maxima are followed towards the solution bulk by a sequence of density maxima, decreasing axially towards the constant value within the reservoirs. The axial ion density profiles are essentially similar to those presented in Fig. 4 of Paper I and feature double layers extending roughly over 7 Å on either side of the membrane and leaving in the reservoirs formed between consecutive replicas of the pore about 14 Å of constant effective bulk concentration. However, there is a qualitative difference in the evolution of the axial ion density profiles with increasing solute density, respectively, increasing applied electric field. The increase of the solute concentration (Fig. 2 upper panel) causes an overall rise of the profiles, predominantly around the double layers, but non-discriminatory on both sides of the membrane. By contrast, the increase of the applied electric field (Fig. 2 lower panel) causes the ion accumulation to be increasingly unbalanced on the two sides of the membrane, with density peaks pronouncedly enhanced for each ion species at the corresponding entrance aperture and diminished on the opposite side. Electrostatically, as proven by the axial potential profiles shown in Fig. 10 and discussed in Sec. III E, the double layers counteract the applied electric field inside the reservoirs screening the pore from its periodic images.

With the exception of the narrow CNTs (8,8) and (9,9), in which the transiting Na^+ ions occupy the central region and both anion species pass on average in the vicinity of the water boundary layer, with increasing channel radius the smaller Cl^- ions pass predominantly closer to the axis switching

positions with the Na^+ ions. As such, a well defined ordering of the density maxima is established for channel chiralities $\geq$ (10,10) and replicated towards the interior depending on the solute type: (H_2O, I^-, Na^+) and, respectively, (H_2O, Na^+, Cl^-). The same patterns can be recognized also in Fig. 1, with the Cl^- and the I^- anions prevailing on the inner and, respectively, outer side of the Na^+ layer. As for the density maximum of Na^+, with minor differences between the NaCl and NaI solutions, it grows significantly when going from 10 ions (dashed line) to 60 ions (continuous line), as expected, but also, to a lesser extent, with increasing axial electric field (lower panel).

The hydrogen atoms can be seen to be located preferentially on the inner side of the water boundary layer, where they optimally hydrate the anions as suggested by the overlap of the hydrogen profiles with those for Cl^- and, respectively, I^-. However, a small excess of hydrogen atoms towards the carbon walls, observed also in the simulations of Peter and Hummer,[7] is also responsible for the net local water polarization (discussed in the following) and for the particular structure of the local electrostatic potential, which is discussed in Sec. III E.

The average radial and longitudinal structuring of the solution can be concisely characterized by the positions of the density peak maxima with respect to the carbon walls. This particular reference is useful to emphasize the practically invariant density patterns, irrespective of the pore radius, the solute concentration, and the applied axial electric field. The density profiles for the total ion numbers from 10 to 60 and applied axial electric fields from 0.005 to 0.05 V/Å illustrate the invariant radial and axial structuring of the solution, yielding as average distances of the density maxima to the carbon walls: 3.20 Å for the water molecules, 5.02 Å for the Na^+ cations, 6.37 Å for the Cl^- anions, and, respectively, 4.14 Å for the I^- anions, with maximum deviations limited by the employed tabulation equidistance of 0.05 Å.

The water structuring in the case of the CNT (10,10) is generally similar to the one produced in the equilibrium pore filling simulations of Nicholson and Quirke.[20] A more illustrative comparison, including the ions, can be made with the radial density profiles reported by Peter and Hummer.[7]

B. Water polarization

The water polarization is defined as ensemble-averaged direction cosine of the electric dipole of the water molecules with respect to the channel axis (electric field direction). Individual ion passages leave pronounced polarization slipstreams and the channel exhibits, as compared to the reservoirs, large polarization fluctuations and a more rapid relaxation due to the smaller number of contained solution components. Technically, the direct binning of the molecular dipole projections according to the distance from the channel axis provides axially cumulated radial water polarization profiles (comprising the integration factor $2\pi r$). *Per molecule* radial profiles of water polarization are there from readily obtained by division by the corresponding radial density profiles.

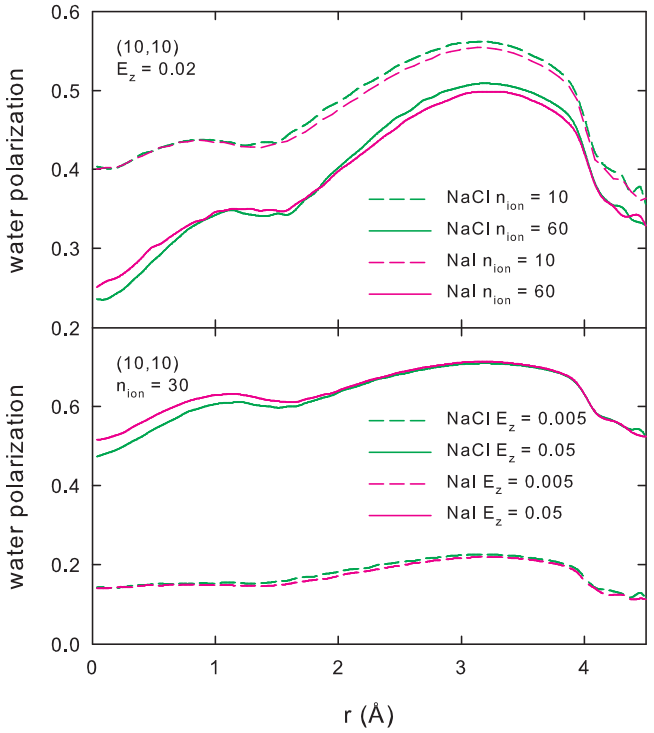

FIG. 3. Per molecule axially averaged radial water polarization profiles inside the CNT (10,10) for representative solute ion concentrations (upper panel) and axial electric fields (lower panel). Dashed lines indicate the lower parameter value.

Representative radial molecular polarization distributions within the CNT (10,10) are shown in Fig. 3 for the minimum/maximum total ion numbers (upper panel) and the minimum/maximum applied axial electric fields (lower panel). The plots are limited to a radial distance of 4.5 Å, beyond which the oxygen density vanishes (Fig. 1). The rather broad polarization profiles follow roughly the water boundary layer and are little depending on the solute type, though feature a slightly more polarizable boundary layer and a slightly less polarizable central region for NaCl as compared to the NaI solution. This behavior results from the comparatively lower Cl^- abundance in the boundary region and the larger concentration near the axis, the solute ions compensating locally the applied electric field and, thus, reducing the average local molecular polarization.

As opposed to the limited anion specificity, the upper panel of Fig. 3 evidences a marked dependence on the solute concentration: lower ion numbers result in more pronounced average polarizations of the water molecules. This inverse dependence of the per molecule polarization on the solute concentration is readily understood again by the depolarizing effect of the solute ions counteracting the applied electric field.

As expected, the lower panel of Fig. 3 confirms the strong dependence of the overall water polarization on the axial electric field. For a tenfold increase of the applied electric field, the maximum water polarization increases nonlinearly more than three times, reaching in the boundary layer values around 0.7, which correspond to average angles formed by the electric dipoles of the water molecules with the channel axis close to 45°.

TABLE I. Average number of NaCl and NaI solution components inside the CNT (10,10) for representative combinations of ion concentrations and axial electric fields.

	n_{ion}	E_z	H_2O	Na^+	Anion	Charge excess
NaCl	10	0.020	164.5	0.74	0.77	−0.03
	30	0.020	164.3	2.07	1.99	+0.09
	60	0.020	165.1	3.55	3.40	+0.14
	30	0.005	165.2	1.06	0.67	+0.39
	30	0.050	166.0	1.97	2.15	−0.18
NaI	10	0.020	163.8	0.86	0.94	−0.08
	30	0.020	164.0	2.17	2.13	+0.04
	60	0.020	166.3	3.65	3.45	+0.20
	30	0.005	166.8	1.28	0.96	+0.32
	30	0.050	166.8	1.81	1.79	+0.02

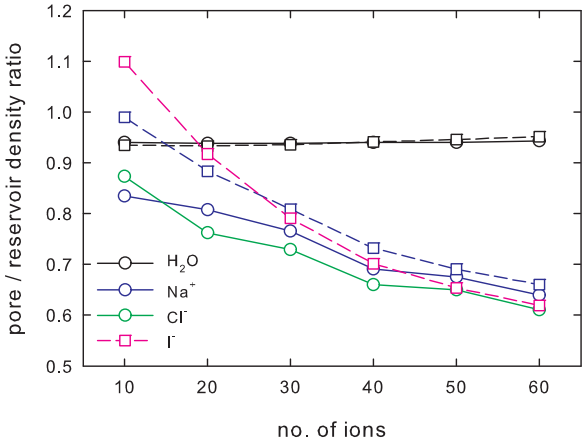

FIG. 4. Pore/reservoir number density ratios for water and solute ions in the CNT (10,10) subject to an axial electric field of 0.02 V/Å as functions of the total ion number. Continuous (dashed) lines correspond to the components of the NaCl (NaI) solution.

C. Pore/reservoir abundances

The straightforward one-dimensional integrals of the radial density profiles of Fig. 1, multiplied by the effective pore length, provide the average numbers of water molecules and solute ions residing inside the CNT (10,10) and actual values for selected concentrations and applied electric fields are listed in Table I. Whereas the number of contained water molecules is influenced indirectly and varies only marginally (by less than 1%), the ion populations are sensitive both to the solute concentration and applied electric field. The superior mobility of the anions (particularly, of I^-), discussed extensively in our next paper,[13] results generally in an excess of "slower" cations inside the CNT. More exactly, the corresponding fractional charge imbalance evolves from a discrete electronegativity for low concentrations to an overall positive charge excess for higher concentrations. In contrast, the increase of the electric field reverses the net positive charge of the pore by the compensating enhancement of the cation mobility.

The ratios between the average densities in the pore and reservoirs offer a complementary picture to the one based on the absolute abundances, not in the least by evidencing the existence of a free energy difference between pore and reservoir ($\Delta F = -k_B T \log(c^{\text{pore}}/c^{\text{res}})$). The concentrations for the pore interior are based on the effective pore volume extending between $\pm z^{\text{eff}}_{\text{pore}}$ and those for the reservoirs are derived from the complementary number of particles and the corresponding volume.

In Paper I, the pore/reservoir density ratios have been shown to increase with the pore radius following approximately the ratio $V^{\text{eff}}_{\text{pore}}/V^{\text{eff}}_{\text{fill}}$ of the effective pore and system volumes (Table III of Paper I). The smooth and roughly parabolic pore radius-dependent profiles for water have been found independent of the solute type and inclusion of molecular polarizability.

The dependences of the pore/reservoir density ratios for the solution components on the total number of solute ions are plotted in Fig. 4. The limited variation for water reflects the already discussed little variation of the absolute populations inside the pore, independently of solute type, with the relative pore densities increasing smoothly from ∼0.95 to the bulk value. The curves for the solute ions, on the contrary, decrease monotonically with increasing total number of solute ions, proving that in relative terms, the increase of the ion density in the reservoirs (predominantly as double layers at the membrane walls) is more substantial than their accumulation in the cylindrical layers inside the pore as shown by the radial profiles of Fig. 1. The *per ion* free energy differences between pore and reservoirs, $\Delta F/n_{ion}$, saturate with increasing solute concentration (already for 40 ions) around 8×10^{-3} kJ/mol.

For a given solute type, the dependences for cations and anions are fairly similar, however with a predominance of anions inside the pore for lower ion concentrations and a prevalence of cations for larger concentrations. The discrete induced charge imbalance is obviously systematic and cannot be considered spurious. As evidenced also by the absolute ion abundances listed in Table I, the trend is more pronounced for NaI than for NaCl, which is in line with the ion-specific selectivity of the CNTs outlined in Paper I.

Figure 5 shows the dependence of the pore/reservoir density ratios of the solution components on the applied axial electric field. Again, the reduced variation of the fraction of water molecules accommodated inside the pore, irrespective of the solute type, is readily visible. The overall effect of the electric field is, nevertheless, to enhance the relative ion population inside the pore, the increase of the fractions for all solute ions having as upper bound the bulk density. The slightly higher density ratios for the intermediate range of applied electric fields (around 0.03 V/ Å) appear to be a consequence of the fact that these fields mark (similar to the role played by the intermediate CNT (10,10) in the discussion of Paper I on the pore radius dependence) the transition from a flow regime with only accidental ion passages for low fields, to a "gating" regime for higher fields. The latter is characterized by alternating, increasingly intense cascades of either cations or anions with typical durations of 1–2 ns, which tend to depopulate the pore and induce a temporarily increased charge imbalance.

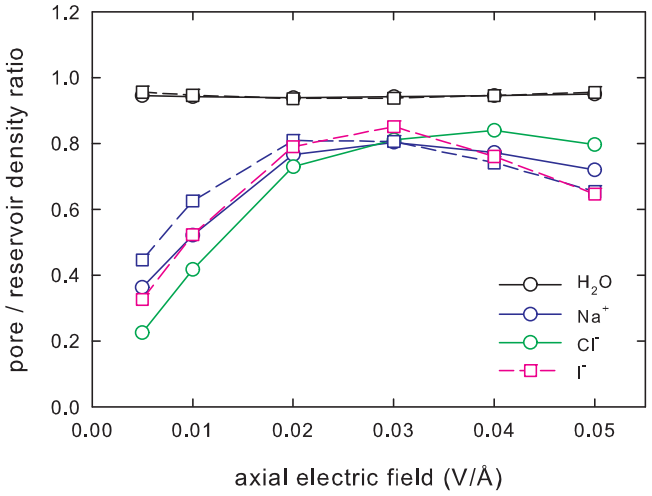

FIG. 5. Pore/reservoir number density ratios for water and solvent ions in the CNT (10,10) as functions of the applied axial electric field. A total of 30 solute ions is considered. Continuous (dashed) lines correspond to the NaCl (NaI) solution.

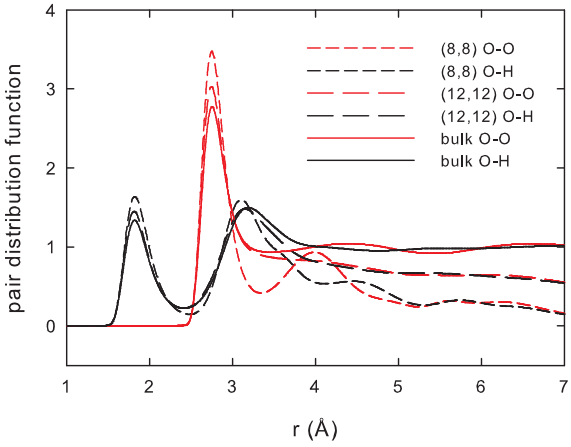

FIG. 6. Radial O–O and O–H distribution functions in the CNTs (8,8) and (12,12) and in the NaCl bulk solution. A total of 30 solute ions and an axial electric field in the CNTs of 0.02 V/Å are considered.

D. Radial distribution functions and coordinations

In addition to the characterization of the solution structuring provided by the radial density profiles, an insightful description of the spherical environment of the solution components inside the pore can be obtained by means of the radial distribution functions[14] (RDFs) and the coordinations derivable there from. Even though the actual compilation of RDFs in systems subject to geometrical constraints (as is the case of CNTs) proceeds, in principle, similar to bulk systems, there is nevertheless a subtle difference, which is sometimes overlooked. Whereas in bulk systems, the RDFs are normalized such that their asymptotic value is 1, as a consequence of the unitary probability to encounter asymptotically a particle under any arbitrary direction, in structured systems (interfaces, nanotubes, etc.) the asymptotic value falls under 1, by a rate depending on the particular geometry. This aspect was grasped, indeed, for instance in the RDFs of Peter and Hummer (Fig. 7 of Ref. 7).

The specific calculation of the RDFs inside the pore is made difficult by the fact that the number of particles (and, implicitly, particle pairs) therein is generally not conserved and that the pore itself is not separately subject to periodic boundary conditions, but jointly with the reservoirs. Technically, the normalization of the RDFs is accomplished by replacing the total simulation cell volume by $V_{\text{eff}} = (4\pi/3)r_{\text{max}}^3(V_{\text{pore}}^{\text{eff}}/V_{\text{fill}}^{\text{eff}})$, where $r_{\text{max}} = \min(x_{\text{cell}}, y_{\text{cell}}, z_{\text{cell}})$ is the sampling radius around any given particle in the pore and the ratios $V_{\text{pore}}^{\text{eff}}/V_{\text{fill}}^{\text{eff}}$ are listed in Paper I. The value of the RDF corresponding to the nth distance bin, defined by $(n-1)\Delta r \le r_{ij} < n\Delta r$, is then

$$g(r_n) = \frac{V_{\text{eff}}}{\sum_n f_n} \frac{f_n}{4\pi r_n^2 \Delta r}, \tag{1}$$

where f_n is the number of particle pairs (i, j) having the distance in the nth bin and $r_n = (n-1/2)\Delta r$ is the corresponding median distance. For a cubic and homogeneous simulation cell, the first factor amounts to $2V_{\text{cell}}/N^2$, with N the total number of particles, and one obtains the formula from standard textbooks.[14]

In order to illustrate more thoroughly the information gained from the RDFs inside the CNTs and, since they have not been discussed in Paper I, besides their dependence on the ion concentration and applied electric field, as pertaining to the subject of the present paper, also the very instructive dependence of the RDFs on the pore radius will be analyzed in the following.

Figure 6 shows the O–O and O–H RDFs inside the narrowest and, respectively, widest of the considered CNTs ((8,8) and (12,12)), along with the RDFs for the corresponding NaCl bulk solution, as references. Whereas for the bulk solution both distributions tend asymptotically to 1, with decreasing pore radius the profiles drop more rapidly and the specific oscillations attenuate (in certain cases, up to the point where a second maximum is no longer recognizable) and shift towards the major peak. At the same time, the magnitude of the major peak increases with decreasing pore radius, as a reflection of the more pronounced confinement of the water molecules in narrower CNTs.

Unlike the monotonic evolution of the major peak magnitudes for the water components with varying pore radius towards the bulk case, the behavior of the Na–O, Cl–H, and I–H RDFs is more nuanced (Fig. 7). An overall increase of the RDFs for the solute ions with increasing pore radius is noticeable, with the profiles for the CNT (12,12) even exceeding somewhat those for the bulk solution and indicating a slightly higher coordination/hydration of the cations/anions in the wider CNTs, but tending to the bulk phase RDFs.

In the considered range of small solute concentrations, the dependence of the RDFs thereon is reduced for all solution components. The Na^+-anion RDFs prove, however, sensitive to the increase of the applied axial electric field and this can be traced back to three, rather pronounced effects: (1) the increase of the average number of ions accommodated by the pore at higher fields (as presented in Table I and discussed in Sec. III C); (2) the increase of the cation/anion counter flows, which make their encounters more probable; (3) the increase

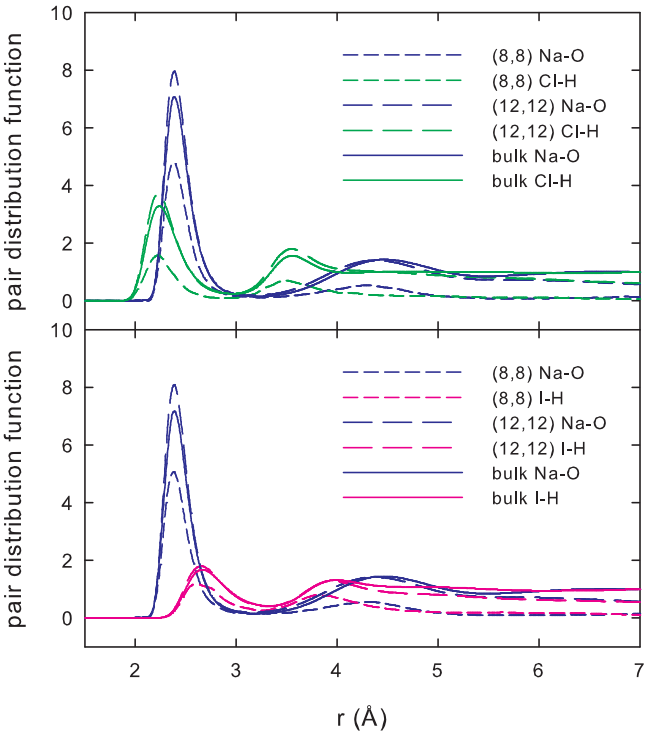

FIG. 7. Radial Na–O, Cl–H, and I–H distribution functions in the CNTs (8,8) and (12,12) and in bulk solutions of NaCl (upper panel) and NaI (lower panel). A total of 30 solute ions and an axial electric field in the CNTs of 0.02 V/Å are considered.

of the water polarization and the consequently stronger correlations between Na^+ and Cl^-/I^-.

With a view to assess the quality of our RDFs, we compare in Table II the main features of our NaCl bulk solution, modeled by a solute ion/water molecule ratio of 30/1000, with the recent results of Mancinelli *et al.*[21] for the solution labeled 1:83, having the closest available ion/water ratio (12/500). The overall consistency and fair agreement in terms of first peak position, first peak magnitude and coordination is readily noticeable. However, a certain disagreement can be identified in the magnitudes of the first peak for Cl^-, which most probably can be ascribed to the use of different water models (TIP4P vs. SPC/E in Ref. 21), slightly different Lennard-Jones parameters for ions and close but different relative ion/water concentrations. Even so, the hydration numbers of the Cl^- anion match perfectly. As for the O–O coordination, our value 4.5 is slightly higher than the standard value 4.4 for bulk water from the literature.[14]

TABLE II. Comparison of the main features of the RDFs for a NaCl bulk solution containing 30/1000 solute ions/water molecules with those of Mancinelli *et al.* (Ref. 21) for a solution with 12/500 solute ions/water molecules (designated as 1:83).

	O–O	Na–O	Na–H	Cl–O	Cl–H
1st peak position	2.75	2.36	2.98	3.13	2.21
Ref. 21	2.75	2.34	2.97	3.15	2.18
1st peak magnitude	2.77	6.87	2.75	3.52	3.21
Ref. 21				3.33	2.46
Coordination	4.5	5.3	13.7	6.5	6.0
Ref. 21		5.3	13.9	6.9	6.0

For the CNT (10,10), it is worth mentioning the agreement of the RDF for Na–O (regarding the position/magnitude of the first peak, asymptotic behavior, and average coordination number) with the results of Peter and Hummer.[7] In particular, the present average coordination number, 5.3, lies well inside the interval [5, 6] reported in the mentioned work, but is slightly higher than the value 4.6 predicted by *ab initio* calculations.[22]

A synthetic characterization of the spherical neighborhood of each solution component is provided by its average coordination (hydration) number. This can be calculated, in principle, as integral over the first (not always major) peak of the corresponding RDF, up to the minimum succeeding it. Whereas the first peak can be always unambiguously identified, the upper limit of integration is sometimes equivocal, especially in cases of systems with constrained geometry, where the above-mentioned decaying asymptotic behavior causes the second peak to become spurious and implicitly the minimum separating it from the first peak to become unrecognizable. Consequently, we have devised a unifying approach to evaluate the coordination, in which the inflection point succeeding the first peak maximum of the RDF is located and the intercept point of the tangent there from with the r axis is used as upper integration limit. The approach was validated for homogeneous bulk systems (featuring a distinct minimum between the first and second RDF peaks), for which the coordination calculated as integral over the first peak up to the intercept point and, respectively, up to the actual minimum have been proven to deviate insignificantly from each other (by less than 0.1%). Nevertheless, the advantage of our tangent-based approach clearly emerges for systems for which a second peak (including a preceding minimum) cannot be identified.

Figure 8 shows the average coordination numbers for O and H (upper panel), as well as for Na^+, Cl^-, and I^- (lower panel) as CNT radius dependences. From the increasing O–O and H-H coordinations, tending to their bulk values (represented as dashed-dotted horizontal lines), and the almost unaffected O–H coordination, one can infer the relatively frustrated neighborhood of the O and H atoms in the narrow channels, which however relaxes rather soon to the bulk situation with increasing pore radius.

While the average number of H–H neighbors appears to be the most affected one in the narrow CNTs (dropping in the CNT (8,8) to almost half its bulk value), the O–O coordination reaches the bulk value already for the CNT (10,10). The quite significant difference of sensitivity to the pore radius found for the H–H and O–O coordinations is consistent with the similar difference for the radial density profiles of the H and O atoms. Relative to the reference radial boundary layer in the CNT (10,10) (Fig. 1), in the CNT (8,8) there is a pronounced broadening for hydrogen (but not also for oxygen), indicating the increasingly outward orientation of the H atoms on both sides of the boundary layer with decreasing pore radius, which obviously leads to the lowering of the H–H coordination. Moreover, this behavior is also consistent with the increase of the water polarization in the radial

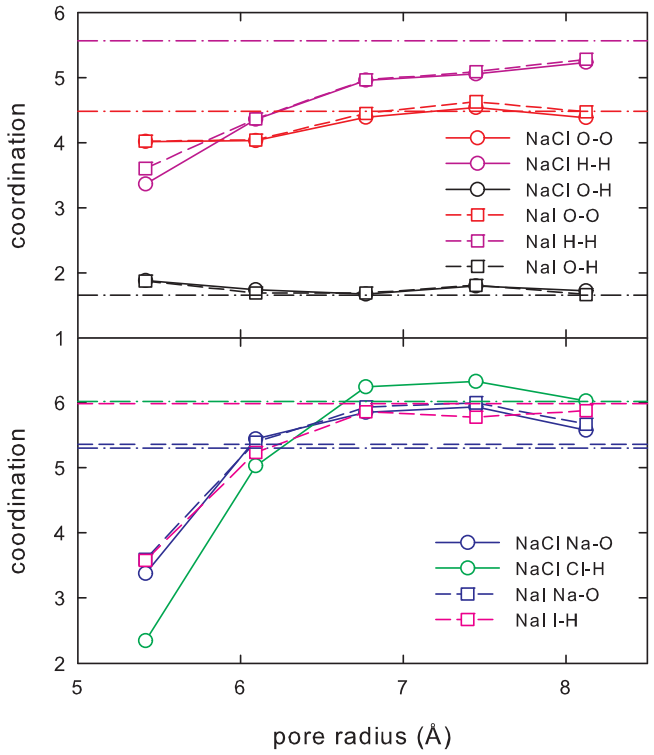

FIG. 8. Average coordinations of the NaCl and NaI solution components as functions of the CNT radius. The reference bulk values are represented with dashed-dotted lines. A total of 30 solute ions and an axial electric field in the CNTs of 0.02 V/Å are considered.

boundary layer with decreasing CNT radius, discussed in detail in Paper I.

The solute ions show fairly similar behavior (lower panel of Fig. 8), with significantly smaller coordinations for the CNT (8,8) and a saturation tendency to the bulk values in the wider nanopores. However, due to its particular radial positioning (Fig. 1), as compared to I^-, the Cl^- anion shows lower hydration in the narrow CNTs and higher hydration in the wider CNTs.

Table III lists, as illustrations of their limited variations, the average coordinations inside the CNT (10,10) for the solution components under the extremal combinations of total solute ion numbers and applied axial electric fields used in the present work. Unlike the invariance found again for O–H, the O–O and H–H coordinations show a slight increase, obviously following the overall increase of the density. On the other hand, the Na–O coordination and the hydrations of the anions, are relatively insensitivity to the solute concentration, showing merely statistical fluctuations about their constant values around 6. A similar relative invariance was found also in the case of the dependences of the coordinations on the applied electric field.

TABLE III. Average coordinations of the NaCl and NaI solution components inside the CNT (10,10) for the extremal combinations of ion concentrations and axial electric fields.

	n_{ion}	E_z	O–O	H–H	O–H	Na–O	Anion–H
NaCl	10	0.020	4.16	5.00	1.79	5.84	6.32
	60	0.020	4.38	5.32	1.63	5.79	6.15
	30	0.005	4.16	4.62	1.71	6.04	6.18
	30	0.050	4.37	5.32	1.64	5.81	6.18
NaI	10	0.020	4.16	4.98	1.72	5.90	5.83
	60	0.020	4.52	5.37	1.66	5.98	6.00
	30	0.005	4.22	5.04	1.72	6.10	6.05
	30	0.050	4.53	5.44	1.79	5.94	5.86

Interesting findings in the particular case of the CNT (10,10) are the overhydration of about 4% of the Cl^- ions with respect to the bulk coordination (as can be seen in Fig. 8) and, moreover, the typical overhydration of 5% with respect to I^-, which is roughly conserved for all considered axial electric fields. The latter finding plays the central role in the explanation given in our next paper[13] on the specific behavior of the NaCl and NaI solutions regarding the net water fluxes driven through the nanochannel by the solute ions in relation to the applied electric field.

E. Electrostatic potential

The detailed structural information provided by the density, polarization, and pair distribution functions presented in the preceding subsections are complemented in the following with information on the structure of the electrostatic field. The electrostatic potential created jointly by the solution components and external fields is obtained, as described in *paper I*, by solving in reciprocal space the Poisson equation for the ensemble-averaged mesh-based charge distribution, $\langle \rho_M(\mathbf{r}_p) \rangle$, which results by projecting the real charge distribution onto a regular three-dimensional grid (used also by the P^3 M Ewald method),

$$\Phi(\mathbf{r}_p) = \overleftarrow{\mathrm{FFT}} \left[\frac{4\pi}{k^2} \overrightarrow{\mathrm{FFT}} [\langle \rho_M(\mathbf{r}_p) \rangle](\mathbf{k}) \right] (\mathbf{r}_p). \tag{2}$$

In Paper I, the anion specificity and the inclusion of molecular and ionic polarizability have been found to have little impact on both the radial and axial electrostatic potential profiles. On the contrary, a significant dependence on the nanotube radius was found and the equally strong dependence on the external electric field will be discussed further. The electrostatic potential profiles shown in Figs. 9 and 10 correspond to the CNT (10,10) filled with NaCl and NaI solutions composed of a total of 30 ions and submitted to the limiting axial electric fields considered here, respectively, 0.005 and 0.05 V/Å.

In the case of the longitudinally averaged radial potential inside the nanopore (Fig. 9), the position of the outer minimum follows essentially the water boundary layer. With increasing electric field, there is an overall lowering of the profiles, as well as an increasing difference between the central minima of the NaCl and NaI solutions. The deeper central minimum for the NaCl solution is obviously a reflection of the pronounced increase of the local radial abundance of Cl^- ions and water seen in Fig. 1. In agreement with Peter and Hummer,[7] the layers of low electrostatic potential coincide with the regions of high oxygen and hydrogen density and the layers of higher electrostatic potential coincide with the regions of low water density.

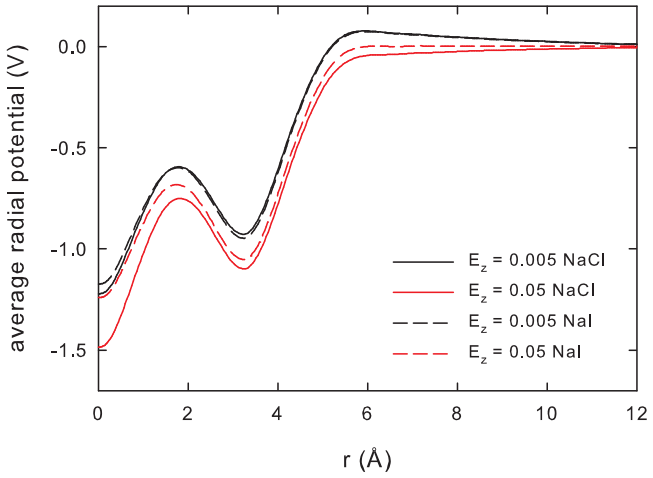

FIG. 9. Average radial electrostatic potential profiles (averaged axially) in the CNT (10,10) for 30 solute ions and representative axial electric fields. Continuous (dashed) lines correspond to the NaCl (NaI) solution.

The transversely averaged axial potential profiles (Fig. 10) show a rather abrupt rise in the reservoirs, marked by oscillations in the region of the water boundary layers and an almost linear decrease inside the nanotube. The potential rise at the channel entrance reflects the formation of a spatial charge (electrochemical double layer) at the membrane walls, which partially neutralizes the applied electric field in the reservoirs. The net height of the electrostatic potential driving the charged particles through the nanotube increases with increasing applied electric field, i.e., the nanotube becomes more permissive to the ion passages, as expected. The profiles for the two non-polarizable solute types are practically identical and slightly bent within the pore.

The variation of the electrostatic potential with the total number of ions is not particularly pronounced over the range of considered concentrations and will be mentioned only in passing. In fact, the effect of the ion concentration on the buildup of charge composing the electrochemical double

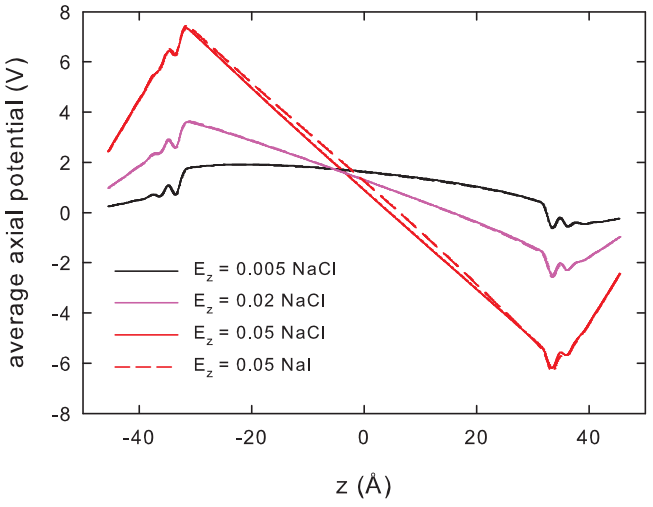

FIG. 10. Average axial electrostatic potential profiles (averaged transversally) in the CNT (10,10) for 30 solute ions and representative axial electric fields. Continuous (dashed) lines correspond to the NaCl (NaI) solution.

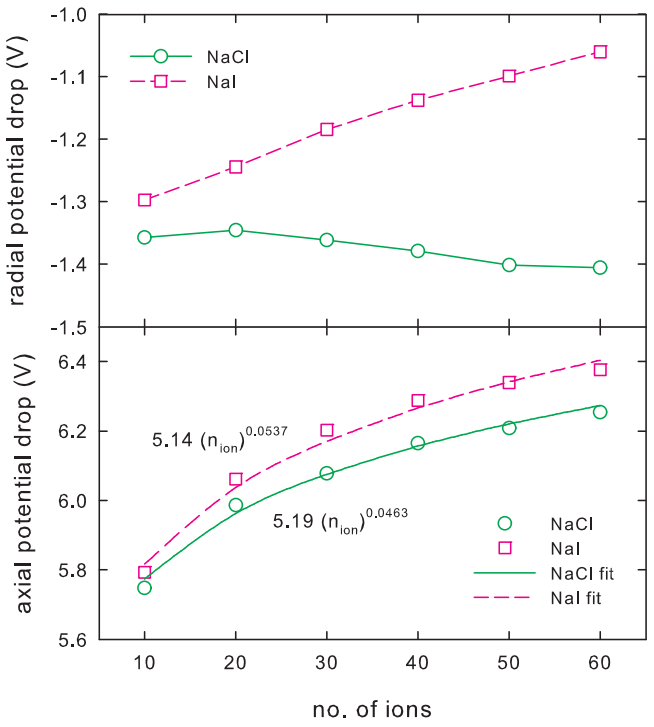

FIG. 11. Average radial and axial electrostatic potential differences for the CNT (10,10), filled with NaCl and NaI solutions and subject to an applied axial field of 0.02 V/Å, as functions of the ion concentration.

layer at the channel apertures is reduced in comparison to the effect of the applied axial electric field. Indirectly, this behavior is an evidence for the significance of the water polarization within the overall electrostatics of the system, which is considerably more sensitive to the applied electric field than to the ion concentration, according to the radial profiles depicted in Fig. 3.

As synthetic indicators for the behavior of the electrostatic potential, Fig. 11 shows the net radial potential well depth (upper panel) and the net axial voltage across the CNT (10,10) (lower panel) as functions of the solute ion concentration. Whereas for the NaCl solution, the concentration increase lowers the central radial potential well due to the accumulation of negative Cl^- ions around the channel axis (see Fig. 1), the central potential drop is seen to reduce for the NaI solution. The ion concentration dependence of the transversely averaged electrostatic potential difference between the channel ends, depicted in the lower panel of Fig. 11, increases and seems to be saturating for both anion species, with the I^- values exceeding by roughly 3% those for Cl^-. To a good approximation, the axial voltage can be represented as a power law of the total ion number (average solute concentration), $\Phi^{\text{axial}} \sim a\langle c_{\text{solute}}\rangle^b$, and the actual fit parameters are specified in Fig. 11.

The net radial potential difference between the periphery and the axis of the CNT plotted in the upper panel of Fig. 12 shows a limited but evidently inverse dependence on the applied electric field. The overall decrease of the potential was already discussed in connection with the radial profiles presented in Fig. 9. The dependence of the transversely averaged electrostatic potential difference along the channel on the

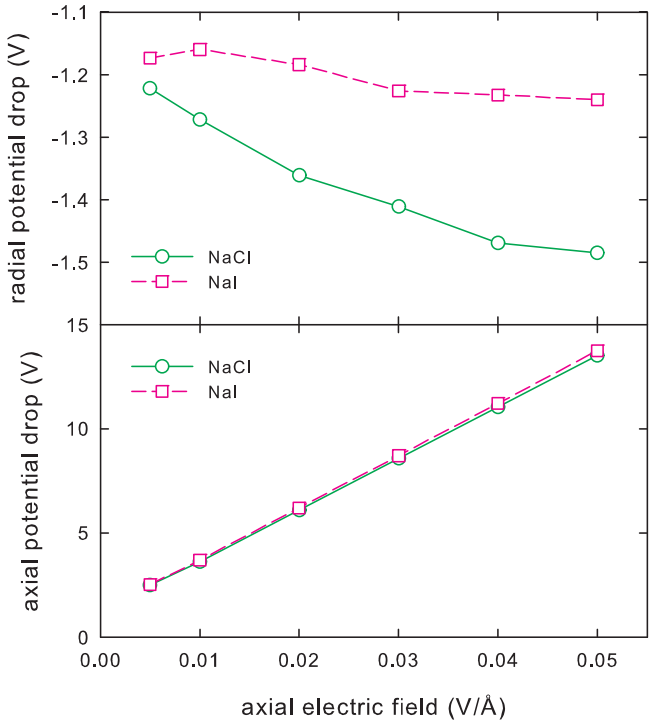

FIG. 12. Average radial and axial electrostatic potential differences for the CNT (10,10), filled with NaCl and NaI solutions composed of 30 ions, as functions of the applied axial electric field.

axial electric field, shown in the lower panel of Fig. 12, is almost linear and clearly insensitive to the solute type. While the potential difference between the two nanopore ends caused solely by the applied electric field amounts to 1.2 V, the transversely averaged potential barriers which have to be overcome by the ions to enter the pore are significantly higher and increase from about 2.5 V to about 13.5 V with increasing axial field. They are clearly a consequence of the formation of electrical double layers at the membrane walls, as discussed before.

A very insightful representation (shown in Fig. 13) is one of the axial potential drops along the CNT for the NaCl and NaI solutions as functions of the axial density maxima of the Cl^- and I^- anions, respectively. The points of each dependence correspond in ascending order to electrostatic fields of 0.005, 0.01, 0.02, 0.03, 0.04, and 0.05 V/Å. This representation reveals the essentially logarithmic dependence of the axial potential barrier on the ratio between the density maximum of cations (anions) at the left (right) channel entrance, $c_{\text{ion}}^{\max}$, and the average density in the reservoirs, $\langle c_{\text{ion}}^{\text{res}} \rangle$,

$$\Phi^{\text{axial}} = a \ln \left(\frac{c_{\text{ion}}^{\max}}{\langle c_{\text{ion}}^{\text{res}} \rangle} \right) - \Phi_0. \tag{3}$$

The actual parameters for the fitting curves depicted in Fig. 13 are $a = 35.8$ and $\Phi_0 = 62.8$ for Cl^- and $a = 15.2$ and $\Phi_0 = 32.0$ for I^- and the concentration independent potential Φ_0 turns out to be of comparable magnitude and to partially compensate the logarithmic term. Similar dependences also hold for the Na^+ cations within the NaCl and NaI solutions.

Interestingly, the logarithmic dependence of the first term of the above model on the maximum concentration in the double layers appears to be similar to the dependence of the Donnan potential on the ion concentration at the bulk-membrane interface $c_{\text{ion}}^{\text{mem}}$ (Donnan[23,24] and Schoch *et al.*[25]),

$$\Phi_D = \frac{RT}{z_{\text{ion}} F} \ln \left(\frac{c_{\text{ion}}^{\text{mem}}}{c_{\text{ion}}^{\text{res}}} \right), \tag{4}$$

where R is the gas constant, T is the temperature, F is the Faraday constant, and z_{ion} is the valency of the ion (± 1). This functional similarity occurs even though the CNTs are characterized by a pronounced solution structuring, with no concentration differences between the reservoirs (due to the periodic boundary conditions), contrasting with the smoothly decreasing concentration profiles inside the permselective membranes and the differing bulk concentrations in the reservoirs, which characterize the models typically described by Donnan potentials.[25] Even though the total axial potential drop Φ^{axial} features a substantial logarithmic (Donnan-type) contribution, the deconvolution of the absolute bulk concentration $\langle c_{\text{ion}}^{\text{res}} \rangle$ as a decaying exponential of Φ^{axial} is hazardous due to the actual domination of the concentration independent potential Φ_0.

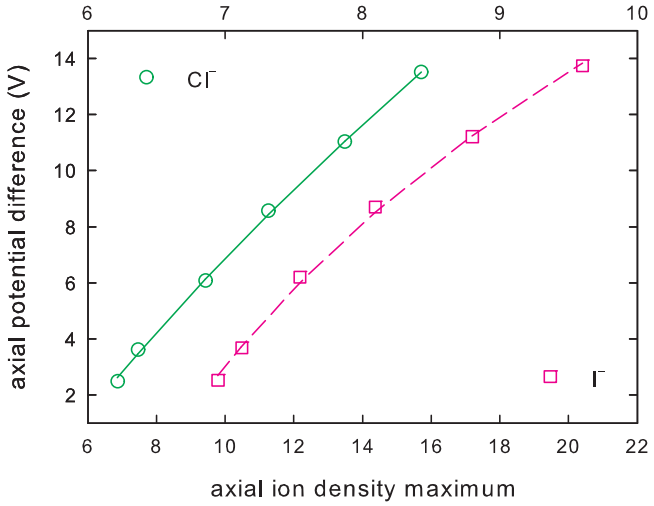

FIG. 13. Axial electrostatic potential difference between the ends of the CNT (10,10) as a function of the axial anion density maximum at the membrane walls for solutions composed of 30 ions. The upper and lower horizontal axes correspond, respectively, to the Cl^- and I^- anions. The continuous curves represent logarithmic fits of the simulation points.

IV. CONCLUSIONS

This second paper in a series dedicated to the systematic MD study of the ion transport through "armchair"-type (n, n) CNTs filled with NaCl and NaI solutions focuses primarily on the effects of the solute concentration and applied external electric fields on the structuring of the solution.

The solutions maintain both inside the channel and near the membrane surfaces an almost invariant structuring (density peak pattern), irrespective of pore radius, solute concentration, and applied axial electric field. Water forms well-defined boundary layers with the hydrogens located preferentially on the inner side, where they optimally hydrate the anions. The effect of the increase of ion concentration and/or

axially applied electric field is to enhance the magnitudes of the density peaks, but not to change their positions.

The pore/reservoir density ratio for the solute ions decreases substantially with increasing total ion concentration, indicating that in relative terms, the accumulation of ions in the reservoirs (predominantly at the membrane walls) is more pronounced than inside the pore. The per ion free energy differences between pore and reservoirs increase, but saturate above 1M to a constant value, which does not show ion specificity. On the contrary, the effect of the electric field is to enhance the relative ion population inside the pore, which is obviously limited by the bulk density.

The RDFs characterizing the average spherical neighborhood of the solution components inside the CNTs agree fairly with radial distributions from the literature in terms of first peak position, first peak magnitude and coordination (in particular, ion hydration). The significant increase of the O–O and H–H coordinations as functions of the pore radius is a reflection of the frustrated neighborhood of the O and H atoms in the narrow nanochannels, which however reaches rather soon (for O–O already within the CNT (10,10)) the bulk conditions. The ions show fairly similar behavior, with significantly smaller coordinations for the CNT (8,8) and a saturation tendency to the bulk values for the wider pores.

The transversely averaged electrostatic potential drop along the CNT can be described to a good approximation by an ion specific *power-law* dependence on the average solute concentration, which can be directly related to the preferential accumulation of ions in the electrochemical double layers with increasing solute concentration, as proven by the radial distributions and the decaying pore/reservoir density ratios. The dependence of the net potential drop along the CNT on the applied axial electric field was found to be linear and the lack of ion specificity can be related to the practically nonspecific character of the corresponding pore/reservoir density ratios. The qualitative difference between the two dependences can be explained by the fact that the increase of the solute concentration causes a general rise of the axial ion density profiles, predominantly around the double layers, but non-discriminatory on both sides of the membrane, whereas, by contrast, the increase of the applied electric field causes the ion accumulation to be increasingly unbalanced on the two sides of the membrane, with density peaks pronouncedly enhanced for each ion species at the corresponding entrance aperture and diminished on the opposite side.

Another noteworthy result is the *logarithmic* dependence of the net axial electrostatic potential difference on the maximum axial density of the various solute ion species. It is a direct indication of the fact that the potential drop across the membrane features a significant Donnan-type contribution, which in turn is determined by the charge build-up and the formation of electrical double layers at the membrane walls.

The structural properties discussed here will be used in the next paper of the series[13] to explain how the solute concentration and the applied electric fields influence the transport properties of the CNTs.

ACKNOWLEDGMENTS

This work was supported by CNCSIS-UEFISCSU, project number PNII-ID PCCE_129/2008.

[1] S. Iijima, Nature (London) **354**, 56 (1991).
[2] *Carbon Nanotubes: Advanced Topics in the Synthesis, Structure, Properties and Applications* edited by A. Jorio, G. Dresselhaus, and M. S. Dresselhaus (Springer, Berlin, 2008).
[3] J. C. Rasaiah, S. Garde, and G. Hummer, Annu. Rev. Phys. Chem. **59**, 713 (2008).
[4] T. A. Beu, J. Chem. Phys. **132**, 164513 (2010).
[5] J. Dzubiella, R. J. Allen, and J.-P. Hansen, J. Chem. Phys. **120**, 5001 (2004).
[6] J. Dzubiella and J.-P. Hansen, J. Chem. Phys. **122**, 234706 (2005).
[7] C. Peter and G. Hummer, Biophys. J. **89**, 2222 (2005).
[8] B. Corry, J. Phys. Chem. B **112**, 1427 (2008).
[9] C. Song and B. Corry, J. Phys. Chem. B **113**, 7642 (2009).
[10] M. Zwolak, J. Lagerqvist, and M. Di Ventra, Phys. Rev. Lett. **103**, 128102 (2009).
[11] M. Zwolak, J. Wilson, and M. Di Ventra, J. Phys.: Condens. Matter **22**, 454126 (2010).
[12] P.-A. Cazade, J. Dweik, B. Coasne, F. Henn, and J. Palmeri, J. Phys. Chem. C **114**, 12245 (2010).
[13] T. A. Beu, J. Chem. Phys. **135**, 044516 (2011).
[14] D. C. Rapaport, *The Art of Molecular Dynamics Simulation* (Cambridge University Press, Cambridge, England, 1995).
[15] R. W. Hockney and J. W. Eastwood, *Computer Simulation Using Particles* (IOP, Bristol, 1988).
[16] M. Deserno and C. Holm, J. Chem. Phys. **109**, 7678 (1998); *ibid.* **109**, 7694 (1998).
[17] W. L. Jorgensen, J. Chandrasekhar, J. D. Madura, R. W. Impey, and M. L. Klein, J. Chem. Phys. **79**, 926 (1983).
[18] M. W. Mahoney and W. L. Jorgensen, J. Chem. Phys. **112**, 8910 (2000).
[19] H. Yu and W. F. van Gunsteren, J. Chem. Phys. **121**, 9549 (2004).
[20] D. Nicholson and N. Quirke, Mol. Simul. **29**, 287 (2003).
[21] R. Mancinelli, A. Botti, F. Bruni, M. A. Ricci, and A. K. Soper, J. Phys. Chem. B **111**, 13570 (2007).
[22] S. B. Rempe and L. R. Pratt, Fluid Phase Equilib. **183**, 121 (2001).
[23] F. G. Donnan, Chem. Rev. **1**, 73 (1924).
[24] F. G. Donnan, J. Membr. Sci. **100**, 45 (1995).
[25] R. B. Schoch, J. Han, and P. Renaud, Rev. Mod. Phys. **80**, 839 (2008).